Available online at www.sciencedirect.com
ScienceDirect
International Journal of Mass Spectrometry 263 (2007) 243–259
International Journal of Mass Spectrometry
www.elsevier.com/locate/ijms

Harmful influences of confinement field non-linearities in mass identifying for a Fourier transform quadrupole ion trap mass spectrometer Simulation studies

Aurika Janulyte, Yves Zerega *, Michel Carette

Université de Provence, Ecole Polytechnique Universitaire de Marseille, Laboratoire IUSTI, UMR CNRS 6595, Equipe Instrumentation de Procédés et Systèmes en Ecoulement, Technopôle de Château-Gombert, F13453 Marseille Cedex 13, France

Received 19 September 2006; received in revised form 26 February 2007; accepted 26 February 2007
Available online 3 March 2007

Abstract

The Fourier transform operating mode applied to a quadrupole ion trap results in an axial secular frequency spectrum of the simultaneously confined ions. During confinement, the ion trajectory must be as pure as possible, giving only one frequency peak for an ion population with the same mass-to-charge ratio.

The simulation work presented here examines the harmful influences of the spatial defects (here, mainly electrode truncation) of the ion trap leading to a non-linear confinement field.

The observed harmful influences on the ion's axial trajectory and its corresponding frequency spectrum is studied based on a case of a single confined ion. Secular frequency of the motion is calculated as a function of the maximum amplitude of the axial and radial trajectories. In the operating mode used in this work, amplitude and frequency of the confinement potential remain constant. As a result, mass analysis is impaired on mass range sustaining the influence of a resonance line. Secular frequency peak amplitude is modified, coupling peaks gain amplitude and ions could be lost. Defective mass ranges have been estimated for a trap truncated at $2r_0$ and $3r_0$ and different maximum amplitudes of the ion motion.

The Fourier transform operating mode requires an external ion source and a large amplitude of the ion motion during confinement. Consequently, even far from a resonance line, ions experience non-linearity effects during confinement due to the maximum amplitude dispersion of the ion cloud during confinement connected to that at the beginning of the confinement. For a same mass-to-charge ratio ion cloud, spectrum is constituted by the superimposition of close-frequency peaks. As a result, mass resolution is limited by peak splitting. In addition to the case of a single confined ion, the operating mode is simulated based on an ion cloud's with initial positions and velocities drawn from Gaussian laws. The mass resolution limit is reported as a function of the initial-condition broadening of the ion cloud. For example, simulation results give a mass resolution of 3250 at the mass 130 u for an operating point $\beta_z = 0.74$ and with an ion cloud having, at the beginning of the confinement for the axial direction, 4 mm for the mean position and 2 mm for the standard deviation.

Keywords: Ion trap; Non-linear field; Secular axial-motion spectrum

1. Introduction

Non-linear resonances in ion traps were first discovered by von Bush and Paul [1] followed by first theoretical and experimental studies carried out by Dawson and Whetten for an ion trap [2] and for a mass filter [3]. An important contribution was made by Wang and Franzen to the understanding of non-linearities by the establishment of mathematical formalisms and by simulation works [4–8].

A non-linear trap is characterised by an electric field whose expression of the radial or axial component is not a linear function of the radial- or axial-position. The observed non-linearities were considered for a long time as defects. They change the motion frequency of the ions when they move away from the trap centre and they can lead to ion losses [9,10]. However, when the ion cloud is "cooled" in the trap centre by a buffer gas (i.e., in a pseudo-thermodynamic equilibrium) these non-linearities are only marginally perceptible by the ions.

Non-linearities are required in ion trap mass spectrometers which operate with voltage amplitude scanning and ion resonant dipolar ejection to increase mass resolution [11]. Ion ejection

* Corresponding author. Tel.: +33 4 91 10 69 23.
E-mail address: yves.zerega@polytech.univ-mrs.fr (Y. Zerega).

1387-3806/$ – see front matter © 2007 Elsevier B.V. All rights reserved.
doi:10.1016/j.ijms.2007.02.048

occurs on a resonance line induced by non-linearity, at a lower voltage operating point than the edge of the stability diagram. At this operating point, ions are submitted to the dipolar resonant excitation (which moves the ions out of the centre) and then to the non-linear resonance effect. Consequently, ejection ion velocity is increased.

In addition to these desired beneficial effects, non-linearities can entail harmful effects such as premature ejections during mass scan and frequency changes [12].

In CID (collision-induced dissociation) experiments, molecular ions are heated and fragmented. Parent ions and daughter ions are in a de-centred position in the trap and then become more sensitive to non-linearities. As a result, losses of ions are observed when the operating point in the stability diagram corresponds to a black hole [13,14] or more generally to zones of bad confinement [15].

Non-linearities are brought about by a modification of the position [16,17] and the shape [18,19] of the electrodes or by the superimposition of an asymmetrical field onto the confinement field [20]. Unexpected non-linearities are induced by imperfections in the construction of the trap, for example, electrodes apertures, electrode truncation, among others [21,22].

Non-linearities are undesirable when the ion trap is used in a Fourier transform quadrupole ion trap mass spectrometer (FTQIT/MS). A significant amplitude of ion motion is necessary to obtain good dynamics of the detected signal [23]. Hence, trajectories can then be strongly disturbed by non-linearities.

In the operating mode used in this study, a periodic signal containing the axial-motion frequencies of the simultaneously confined ions is obtained [24]. A Fourier transform of this signal gives the spectrum. Peak frequency and amplitude are representative of the ion population depending on their mass-to-charge ratio and their abundance, respectively.

Axial-motion frequencies of an ion confined in a pure quadrupole trap are given by

$$\pm\omega_z + n\Omega, \quad \text{with } n \text{ integer} \tag{1}$$

In Eq. (1) above $\omega_z = \beta_z\Omega/2$ is the secular frequency of the axial-motion. The β_z defines the ion trap operating point and depends on the following parameters: $U_0 + V_0\cos(\Omega t + \varphi_i)$, the dc and ac potentials applied to the ring electrode, the two end-caps being earthed; z_0, the distance separating the trap centre and one end-cap along the Oz axis; and m/z, the mass-to-charge ratio of the ion.

If the function describing the ion trajectory is sampled at Ω, frequencies greater than $\Omega/2$ fold over in the range $[0, \Omega/2]$ at ω_z, the secular frequency peak [25]. As a result, only one peak is observed, which makes mass identifying easy.

Different physical phenomena can lead to peak enlargement and/or peak addition which impair mass analysis (resolution, signal-to-noise ratio and mass identification).

Ion collisions with a background gas lighter than the trapped ions reduce ion trajectory amplitude during confinement. Such phenomena can be modelled by an exponential decreasing of the motion amplitude. Consequently, the frequency peak obtained with a Fourier transform has a Lorentzian shape, i.e., its base is enlarged. For example, under normal operating conditions at a pressure $p \approx 10^{-7}$ Torr inside the trap, ion collisions lead to an enlargement of the full width at half maximum of about 10 Hz [26]. The additional dephasing in the trajectory induced at each collision entails only background noise in the spectrum. Hence, ion creation is performed outside the mass-analysis trap.

Defects of the electric confinement field (such as a superimposition of a sinusoidal voltage in a quadrupolar configuration on the confinement voltage) induce coupling peak. Indeed ion motion is modulated at the frequency of the supplementary voltage. The amplitude of the modulation is inversely proportional to this frequency. Therefore, the power supply frequency (50 Hz) must be filtered. With the Fourier operating mode, an additional phase modulation can occur depending on the repetition time of the elementary experiments [27]. For example, to reach a mass resolution of about 5600 at the mass 130 u, the amplitude of the supplementary voltage (induced by the power supply) must be lower than 20 mV.

Spatial defects of the ion trap – electrode truncation, electrode displacement and apertures in the two end-caps – lead to a non-linear confinement field. In this operating mode, the first harmful effect is that secular frequency depends on maximum amplitude of the ion motion as confinement initial conditions are spread. Coupling peaks gain amplitude when the operating point is located near a resonance line that impairs mass identifying. Ion loss could happened by trajectory extension if operating point is close to a resonance line. Mainly non-linearities induced by electrode truncations are concerned in this study. First, all these effects will be studied according to some experimental parameters for only one confined ion. Then resolution limit of the operating mode will be estimated for an ion cloud depending on its dispersion and on the trap truncation.

2. Theoretical developments

Potential inside the trap is the solution of the Laplace equation. A general solution is given by

$$\phi(\rho, \theta, \varphi, t) = \sum_{n=0}^{+\infty} C_n \rho^n P_n^m(\cos\theta)\cos m\varphi \tag{2}$$

where $P_n^m(\cos\theta)$ is a Legendre polynomial and C_n is a coefficient which depends on boundary conditions.

We consider that the deformations and/or displacements of the trap electrodes causing non-linearities keep the axial (Oz) and radial (the plane xOy) symmetries which exist in the case of a pure quadrupolar trap. Thus, the expression of the electric potential does not depend on the variable φ, which imposes $m = 0$. And the terms of order n of odd value are null. Such a potential can be generated only by an even number of charges. Moreover, the deformations and/or displacements of the electrodes are considered not modify the smallest radius of the ring $r_0 = \sqrt{2}z_0$ located at the dimension $z = 0$ in the radial plane xOy.

The potential in Cartesian coordinates is expressed by

$$\phi(x, y, z, t) = \phi_0(t)\sum_{p=0}^{+\infty} A_{2p}\left(\frac{\rho}{r_0}\right)^{2p} P_{2p}^0(\cos\theta) \tag{3}$$

In Eq. (3) above $\rho = \sqrt{x^2 + y^2 + z^2}$, $z = \rho\cos\theta$, $\phi_0(t) = U_0 + V_0\cos(\Omega t + \varphi_i)$ is the potential applied to the ring electrode located at r_0 in the radial plane xOy at $z = 0$ and A_{2p} is a coefficient which depends on the boundary conditions.

Written in this form, one can use the values of these coefficients calculated for certain types of non-linearities by Wang and Franzen [6].

By developing the first two terms of the sum, the potential is expressed by

$$\phi(x, y, z, t) = \phi_0(t)\left[A_0 + \frac{A_2}{2}\left(\frac{2z^2 - (x^2 + y^2)}{r_0^2}\right) + \sum_{p=2}^{+\infty} A_{2p}\left(\frac{\rho}{r_0}\right)^{2p} P_{2p}^0(\cos\theta)\right] \tag{4}$$

For a pure quadrupolar (linear) trap, $A_2 = 1$ and all the other terms are null. Non-linearity is characterised by the values of the coefficients A_n for $n \geq 2$. In general, for small displacements or slight shape-modifications of the electrodes, these coefficients are very small in relation to A_2.

The ion motion equations are taken from the fundamental equation of dynamics. The equations according to directions Ox and Oy of the radial plane are identical. Thereafter only the expression of the equation according to the direction Ox will be given.

Given that

$$\Omega t = 2\tau, \qquad a_z = -2a_x = -2a_y = +\frac{8ZeU_0}{m\Omega^2 r_0^2},$$
$$q_z = -2q_x = -2q_y = -\frac{4ZeV_0}{m\Omega^2 r_0^2} \tag{5}$$

the ion motion equation on the Ox axis is obtained by

$$\frac{\mathrm{d}^2x}{\mathrm{d}\tau^2} = (a_x - 2q_x\cos 2\tau)r_0^2 \times \left[\frac{A_2}{2r_0^2}(-2x) + \frac{A_4}{8r_0^4}(-48z^2x + 12xr^2) + \frac{A_6}{16r_0^6}(-240z^4x + 360z^2xr^2 - 30xr^4) + \frac{A_8}{128r_0^8}(-18,038z^6x + 13,440z^4xr^2 - 6720z^2xr^4 + 280xr^6) + \frac{A_{10}}{3840r_0^{10}}(-172\,800z^8x + 1,209\,600z^6xr^2 - 1,512\,000z^4xr^4 + 378\,000z^2xr^6 - 9450xr^8)\right] \tag{6}$$

The axial direction Oz is given by

$$\frac{\mathrm{d}^2z}{\mathrm{d}\tau^2} = -(a_z - 2q_z\cos 2\tau)\frac{r_0^2}{2} \times \left[\frac{A_2}{2r_0^2}(4z) + \frac{A_4}{8r_0^4}(32z^3 - 48zr^2) + \frac{A_6}{16r_0^6}(96z^5 - 480z^3r^2 + 180zr^4) + \frac{A_8}{128r_0^8}(87,512z^7 - 54,114z^5r^2 + 13,440z^3r^4 - 2240zr^6) + \frac{A_{10}}{3840r_0^{10}}(38,400z^9 - 691\,200z^7r^2 + 1\,814\,400z^5r^4 - 1\,008\,000z^3r^6 + 94,500zr^8)\right] \tag{7}$$

with $r = \sqrt{x^2 + y^2}$. The ion motion equations are coupled for non-linear traps unlike the pure quadrupole trap.

The motion spectrum is comprised of frequency peaks of the pure quadrupolar trap at lower frequencies due to $A_2 \leq 1$. Other frequency peaks appear in the spectrum: harmonic peaks of the secular motion for each direction and coupling frequency peaks between axial and radial directions.

The non-linearities introduce resonance lines inside the principal stability diagram. These resonances result from couplings, on the one hand between the direction Oz and a direction of the plane xOy (for the terms of the motion equations in $z^l x^m y^n$), and on the other hand between a direction of the space and the excitation field (for the terms of the motion equations in z^l, x^m and y^n). Franzen et al. [28] present a very interesting set of figures locating in the plane (β_r, β_z) the resonance lines for the poles of orders $n = 3$–10.

In the case of the adiabatic approximation, i.e., for $a_z = 0$ and $q_z \leq 0.4$, for a non-linear ion trap with solely $A_2 \neq 0$ and $A_4 \neq 0$, and without ion displacement in the radial plane, $Z_s(t)$, the secular axial-motion is given by [11]:

$$\frac{\mathrm{d}^2Z_s(t)}{\mathrm{d}t^2} + \frac{\Omega^2}{8}q_z^2A_2^2Z_s(t) = -\Omega^2q_z^2\frac{A_2A_4}{r_0^2}Z_s^3(t) \tag{8}$$

By using a perturbation method, an approximate solution is written in the follow form [29]:

$$Z_s(t) \approx z(t_0)\cos\omega_z' t + \frac{z^3(t_0)}{4r_0^2}\frac{A_4}{A_2}\cos 3\omega_z' t + \cdots \tag{9}$$

where,

$$\omega_z' \approx \frac{\Omega|q_z|}{2\sqrt{2}}\left(A_2 + 3\frac{A_4}{r_0^2}z^2(t_0) + \cdots\right) \tag{10}$$

In Eqs. (9) and (10) above, $z(t_0)$ is the axial-position at the beginning of the confinement. The initial axial velocity $v_z(t_0)$ must be equal to zero. For non-linearities having even-order multipolar terms, the equation of the axial-motion comprises odd values of

powers of $z(t)$. The solution of this equation is described by a function with null average value.

Eq. (10) listed above shows that the non-linearities introduce modifications of the fundamental frequency [30]. If a coupling term exists between the axial direction and a radial direction in the motion equation, the frequency is a function of the radial initial conditions of the ions. Consequently, in the case of non-linearities, the motion frequency depends on the operating point, the multipolar terms A_n and the initial conditions of the ions.

3. Ion trap operating mode

3.1. Description

The Fourier transform quadrupole ion trap operating mode requires a set of N elementary experiments. An elementary experiment consists of the following stages Fig. 1:

(1) Creation: the ions are created in the source by a pulsed electron beam.
(2) Injection: the ions are introduced into the trap and are slowed down by static electric fields.
(3) Confinement: the confinement field is turned on at t_0 and the ions are thus confined during t_i. i is the index of the confinement time and of the elementary experiment. The confinement voltage $U_0 + V_0 \cos \Omega t$ is applied to the ring electrode. Its amplitude and frequency remain constant during confinement.
(4) Ejection: the confinement field is then replaced by a static field which moves the ions towards a fast response electron multiplier.
(5) Measurement: the electron multiplier delivers an electric signal that is sampled and recorded. The resulting signal is called a time-of-flight (TOF) histogram. The TOF is the time that the ion spends to cover the distance between its position in the trap at the end of confinement and the first dynode of the electron multiplier. The histogram area is proportional to the total number of collected ions. The mean value and the spread of TOF histograms depend on the ion cloud positions and velocities at the end of the confinement duration t_i.

Since the measurement is destructive, this elementary experiment is reproduced for a set of N confinement times $\{t_i = iT_e, i = 1\text{–}N\}$. $T_e = jT_\Omega$ is the sampling period. Generally, $j = 1$. In experiments j can be chosen greater than 1 to increase resolution. In this simulation work a j value lower than 1 will be chosen to increase the observation frequency range to reduce peak fold over.

3.2. Signal treatment

The TOF histogram treatment leads to a periodic function versus t_i the frequencies of which are the axial secular frequencies of the simultaneously confined ions. The motion spectrum is obtained by a Fourier transform of this function [31,24].

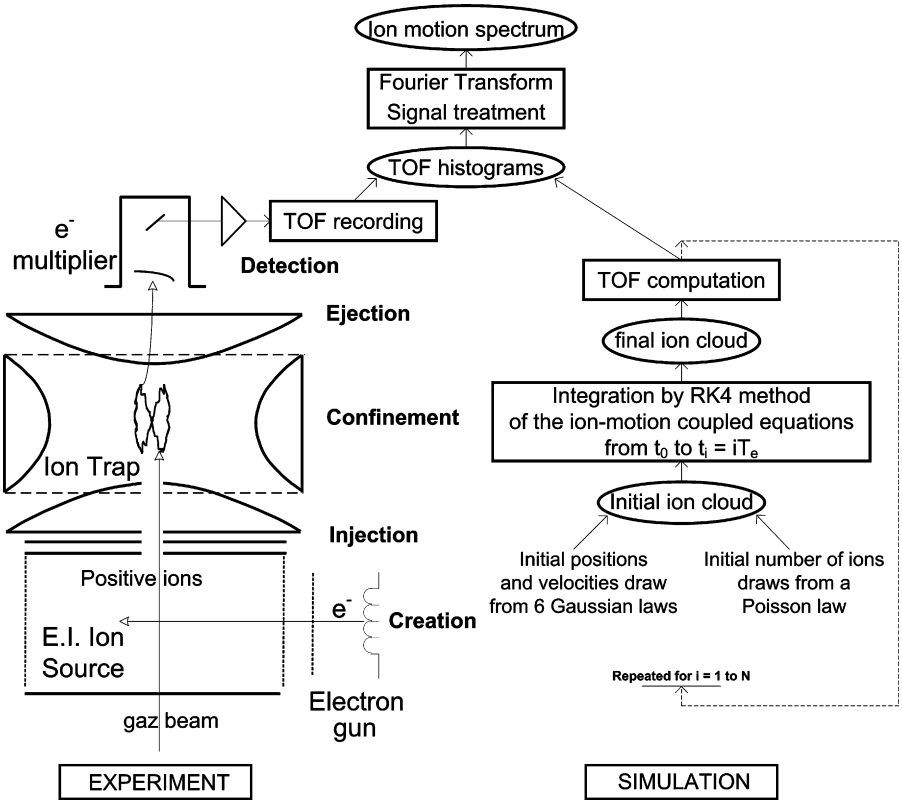

Fig. 1. EI ion source and ion trap mass analyser. Description of the elementary experiment stages and corresponding simulation stages. The TOF histogram treatment is the same for experimental and simulation results.

Measured signals are periodic: they present a line spectrum. The magnitude spectrum of a periodic signal, observed during $T_m = NT_e$, comprises peaks of the form $|\mathrm{sinc}(\pi\nu T_m)|$. Such shape exhibits auxiliary wiggles on both sides of the main peak. The relative amplitude of the side wiggles is 22% for the amplitude spectrum. Such wiggles make it difficult to observe a small peak near a large peak. Multiplying the temporal signal by an apodization function (for example, here, by an exact Blackman function), reduces the wiggle amplitude. The relative amplitude of the higher wiggles is then 0.04%. However, the main peak becomes wider.

Sampling the temporal signal at the period T_e limits the frequency exploration to the range $[0, 1/(2T_e)]$ (Shannon or Nyquist theorem). Larger frequency peaks fold over at false frequency values in this domain.

Discrete Fourier transform (DFT) algorithms give a discrete spectrum whose frequency step is $\nu_m = 1/T_m$. This step is not sufficient to reveal the exact shape of the peak as its base width is equal to $2/T_m$. Before performing DFT, zeros are added to the temporal signal (zero filling or padding) to reduce the frequency step in the spectrum [25]. Frequency step of the computed points is expressed by $\nu_m = 1/T'_m$, where $T'_m = N'T_e$, where N' is the number of temporal points after zero addition (we chose five zero additions). If N is a power of two then $N' = 32N$. Otherwise, N' is chosen to equal the nearest superior value of N^2 multiplied by 16. For example, with $N = 1000$, $N' = 1024 \times 16 = 16\,384$ and the frequency step is about 15.25 Hz and for $N = 20\,000$, $N' = 32\,768 \times 16 = 524\,284$ and the frequency step is about 0.48 Hz.

With such frequency step, choosing the maximum amplitude of the peak to locate the peak frequency results in a sufficiently accurate measurement.

3.3. Resolution

By Fourier analysis, $\delta_{1/2,\nu}$, the full width at half maximum (FWHM) of the peak, is expressed by

$$\delta_{1/2,\nu}\,(\mathrm{Hz}) = \frac{\alpha}{T_m} \tag{11}$$

Without an apodization function, $\alpha \approx 1.2$ for the magnitude spectrum and 0.89 for the power spectrum. By using the exact Blackman apodization function before performing Fourier analysis, $\alpha \approx 2.24$ for the magnitude spectrum and 1.6 for the power spectrum. The benefit of this apodization function is that it greatly reduces noise level and also induces a peak enlargement. To have a lower peak enlargement, a Hamming apodization function is used: $\alpha \approx 1.81$ for the magnitude spectrum and 1.3 for the power spectrum, but the relative amplitude of the higher wiggles is 0.75%, which increases the noise level.

In the operating mode used here, mass resolution depends on the operating point [26]. As mass analysis is performed with V_0 constant, for example for two ions different in m/z ratio, the higher the operating point, the larger the difference frequency between the two ions.

Table 1
Mass FWHM computed from Eq. (12) for magnitude and power frequency spectra for three operating points with $N = 1000$

V_0 (V)	ω_z (kHz)		Δ_{ω_z} (Hz)	$\delta_{1/2,m/z}$ (u)	
	130 u	131 u		Magnitude	Power
45	24.283	24.093	190.5	2.94	2.105
108.35	64.054	63.43	624	0.898	0.643
138	92.060	90.727	1333	0.420	0.301

The axial secular frequency ω_z is measured from spectra computed with the following conditions: one ion confined in a $3r_0$ truncated trap, an exact Blackman apodization function, $\Omega/2\pi = 250$ kHz, $z_0 = 1$ cm, $U_0 = 0$ V, $T_e = T_\Omega = 4$ μs, $N = 20\,000$, $z(t_0) = -2$ mm and $x(t_0) = y(t_0) = 0$ mm.

Mass FWHM of the peak can be expressed by

$$\delta_{1/2,m/z}\,(\mathrm{u}) = \delta_{1/2,\nu}\frac{\Delta_{m/z}}{\Delta_{\omega_z}} \tag{12}$$

where Δ_{ω_z} is the axial-secular frequency difference between two ions with a mass difference equal to $\Delta_{m/z}$. The Δ_{ω_z} increases with the increasing of V_0, as does mass resolution too.

Table 1 gives the mass FWHM of the peak for three operating points. With an exact Blackman apodization function and $N = 1000$, Eq. (11) gives $\delta_{1/2,\nu} = 560$ Hz for the magnitude spectrum and 401 Hz for the power spectrum. The frequency difference Δ_{ω_z} is computed from the secular frequency trajectory of two ions with a mass of 130 and 131 u.

The magnitude spectrum is drawn in figures to show a linear behaviour of the peak amplitude. To obtain a better resolution, the FWHM is computed from the power spectrum.

Remaining side lobes are the sole noise source when only one ion trajectory is considered which is the case in the first part of the results.

4. Modelling of the experiment

4.1. Initial conditions

The initial moment t_0 of the simulation is fixed at the beginning of the confinement. Ion injection is not taken into account.

Initial ion positions $x(t_0)$, $y(t_0)$, $z(t_0)$ and initial ion velocities $v_x(t_0)$, $v_y(t_0)$, $v_z(t_0)$ are drawn from six Gaussian laws of parameters: $(\bar{x}(t_0), \sigma[x(t_0)])$, $(\bar{y}(t_0), \sigma[y(t_0)])$, $(\bar{z}(t_0), \sigma[z(t_0)])$, $(\bar{v}_x(t_0), \sigma[v_x(t_0)])$, $(\bar{v}_y(t_0), \sigma[v_y(t_0)])$ and $(\bar{v}_z(t_0), \sigma[v_z(t_0)])$, respectively.

The injection mode imposes the following choice of initial conditions for the confinement stage:

- On the radial plane, the ion cloud is centred: $\bar{x}(t_0) = \bar{y}(t_0) = 0$ mm. Its standard deviation is twice as large as the injection aperture: $\sigma[x(t_0)] = \sigma[y(t_0)] = 2$ mm.
- On the radial plane, the ions of the cloud have a slight velocity spreading over: $\bar{v}_x(t_0) = \bar{v}_y(t_0) = 0$ m/s and $\sigma[v_x(t_0)] = \sigma[v_y(t_0)] = 300$ m/s.
- On the Oz axis, the ion cloud is stopped in a de-centred position before the centre of the trap. In simulation, $\bar{z}(t_0)$ varies

between 0 and −6 mm with a standard deviation of the ion cloud $\sigma[z(t_0)]$ ranging between 2 and 4 mm.
- On the Oz axis, the average velocities are null $\bar{v}_z(t_0) = 0$ m/s. The standard deviation of velocities is more significant than on the radial plane, because the ion translation is carried out according to the Oz axis.

The number of ions injected N_i is drawn from a Poisson law of parameter $\bar{N}_i$, the mean number of ions per experiment.

4.2. Confinement

Ion positions $x(t_i)$, $y(t_i)$ and $z(t_i)$ and velocities $v_x(t_i)$, $v_y(t_i)$ and $v_z(t_i)$ (at the end of the confinement time t_i) are computed from trajectories given by Eqs. (6) and (7) by an RK4 numerical method with 1200 points per period of the ac confinement voltage.

The initial phase of the confinement voltage φ_i is chosen equal to π. In this case, in a pure quadrupolar ion trap, with an initial velocity equal to zero, the maximum extension of the axial trajectory is equal to the initial axial-position.

Simulations are carried out for a pure quadrupolar trap and for three types of non-linearities: a stretched trap, a trap truncated at $2r_0$ and another at $3r_0$. The stretched trap is integrated in the mass spectrometers of the Finnigan MAT company. The non-linear fields introduced by the stretch are used to offset the field faults caused by the holes in the end-caps [32].

In the FTQIT mass spectrometer, non-linear fields come from apertures, missed-alignment and truncation of the electrode. Here, only the last perturbation is taken into account. The electrodes are truncated at the dimension $2r_0$ (or $3r_0$) on each asymptote of the potential separating an end-cap from the ring. They keep the cylindrical symmetry of the electrodes. For each type of non-linearity, coefficients A_{2p} are given by Wang and Franzen [6] and are limited to $2p = 10$.

4.3. Ejection

At the end of the confinement, the ions are ejected out of the trap and are directed towards the electron multiplier. We consider that the time-of-flight to reach the multiplier is negligible in comparison with the time that it takes the ion to leave the trap (at the dimension z_0). It is supposed that the electrical field inside the trap at ejection is dipolar. Hence TOF versus time of confinement is expressed by [31]:

$$t_f(t_i) = \frac{1}{A\left[-v_z(t_i) + \sqrt{v_z^2(t_i) - 2A(z(t_i) - z_0)}\right]} \quad (13)$$

where $A = (ZeU_e)/(mz_0)$, with $2U_e$ being the voltage applied between the two end-caps during the ejection stage.

Then, a TOF histogram is built for the confinement time t_i. As in experiment, a set of elementary experiments are performed for increasing confinement times and a same treatment is applied to the set of histograms to obtain motion frequency spectrum of the simultaneously confined ions.

5. Results and discussion

5.1. Preliminaries for a single ion treatment

In the operating mode, mass identifying is performed from the spectrum of a periodic signal function of positions and velocities during confinement. In consequence, non-linearity influences of the trap can be gauge from the axial spectrum of only one confined ion, which will be done in a first time in the two next paragraphes. In this case, to obtain the spectrum, signal treatment (apodization, zero padding and Fourier transform) is applied on a same axial trajectory computed for each t_i (i varying between 1 and N) with $x(t_0)$, $y(t_0)$, $z(t_0)$, $v_x(t_0)$, $v_y(t_0)$ and $v_z(t_0)$ as initial conditions.

5.2. Axial-motion secular frequency versus initial position

In the FTQIT operating mode, ions have large and different motion amplitudes during confinement. Hence, influence of the initial conditions (directly connected to the maximum amplitude of the ion motion, as initial velocity is null) on the secular frequency is examined in the case of one ion.

5.2.1. Versus initial axial-position

Fig. 2 shows the frequency variation of the secular axial-motion versus $z^2(t_0)$ for the three types of non-linear ion traps. Trap operating points (depending on V_0) are chosen far from a resonance line in order to obtain only the axial secular frequency peak without any significant coupling peaks.

The secular axial-motion frequency of an ion confined in a trap truncated at $2r_0$ is lower than that of an ion confined in a trap truncated at $3r_0$, which is lower than that of an ion confined in pure quadrupolar ion trap.

In the case of truncated ion traps, the frequency decreases with the increasing of $z^2(t_0)$ as A_4 is negative (Eq. (10)). This decrease is not linear as expected in this equation. This approximate equation does not take into account A_6, A_8 and A_{10} which are negative for the two truncated ion traps. For example, A_6 adds a new term which is proportional to $A_6 z^4(t_0)$. Consequently, the curves of Fig. 2 present a decrease greater than a linear decrease.

For a stretched ion trap, the frequency increases with the increasing of $z^2(t_0)$ as A_4 is positive. This increase is not linear as expected in Eq. (10). For example, A_6, which is positive for a stretched ion trap, adds a new term which is proportional to $A_6 z^4(t_0)$. Consequently, the curve presents an increase greater than a linear increase.

5.2.2. Versus initial radial-position

Fig. 3 shows the frequency variation of the secular axial-motion versus $r^2(t_0) = x^2(t_0) + y^2(t_0)$ for an ion trap truncated at $2r_0$ and $3r_0$. x is equal to y and both vary between 0 and 6 mm in steps of 1 mm.

Here, a coupling between the axial and the radial directions exists because $x(t_0) = y(t_0) \neq 0$. A_4 induces a secular frequency increase proportional to $r^2(t_0)$, while A_6 induces a secular frequency increase proportional to $r^2(t_0)$ and $z^2(t_0)$ and a decrease proportional to $r^4(t_0)$.

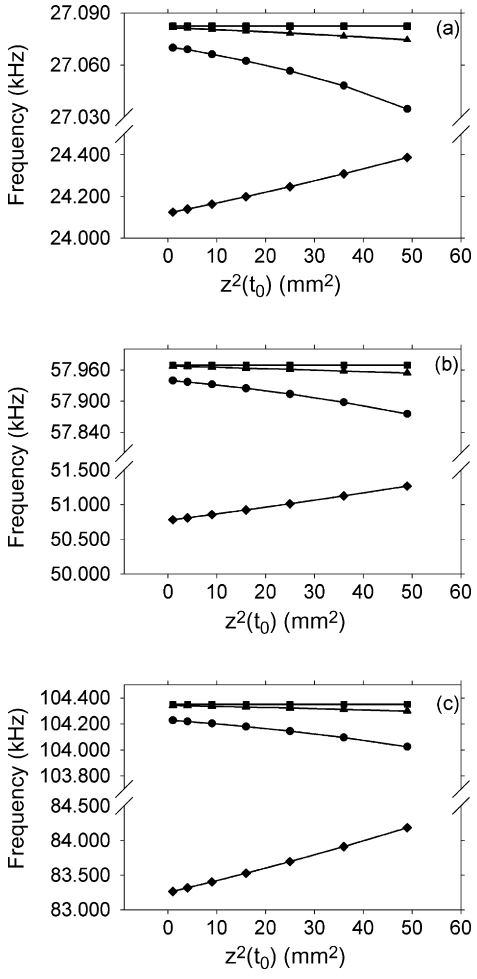

Fig. 2. Frequency of the secular axial-motion peak of an ion confined in: (square) a pure quadrupolar trap; (triangle) a trap truncated at $3r_0$; (circle) a trap truncated at $2r_0$ and (diamond) a stretched ion trap vs. $z^2(t_0)$ with (a) $V_0 = 50$ V, (b) $V_0 = 100$ V and (c) $V_0 = 145.8$ V. The other conditions are: $m/z = 130$ u, $\Omega/2\pi = 250$ kHz, $z_0 = 1$ cm, $U_0 = 0$ V, $T_e = T_\Omega = 4$ μs, $N = 20\,000$ and $x(t_0) = y(t_0) = 0$ mm.

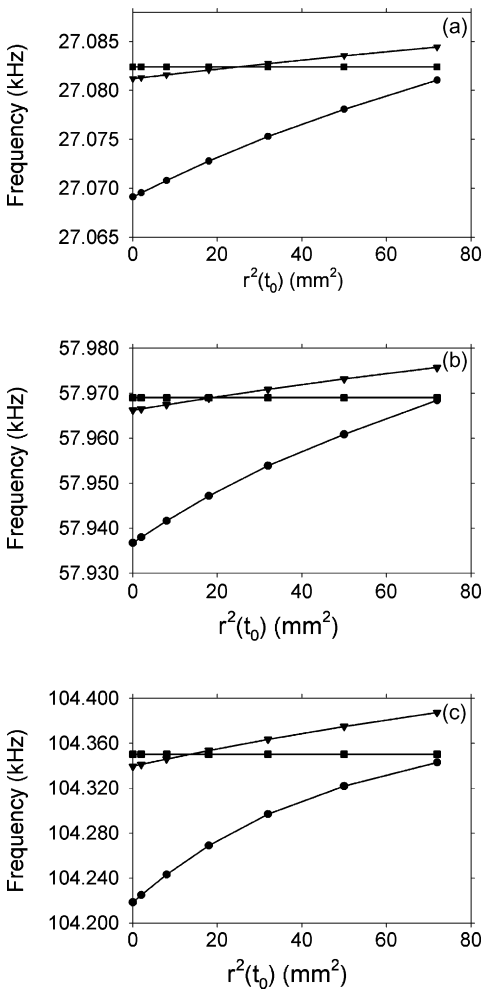

Fig. 3. Frequency of the secular axial-motion peak of an ion confined in: (square) a pure quadrupolar trap; (triangle) a trap truncated at $3r_0$ and (circle) a trap truncated at $2r_0$ vs. $r^2(t_0) = x^2(t_0) + y^2(t_0)$ with (a) $V_0 = 50$ V, (b) $V_0 = 100$ V and (c) $V_0 = 145.8$ V. The other conditions are: $m/z = 130$ u, $\Omega/2\pi = 250$ kHz, $z_0 = 1$ cm, $U_0 = 0$ V, $T_e = T_\Omega = 4$ μs, $N = 20\,000$ and $z(t_0) = -2$ mm.

In Fig. 3, for a trap truncated at $3r_0$, as A_6 is negligible, the frequency increases almost in proportion to $r^2(t_0)$. For a trap truncated at $2r_0$, a decrease proportional to $A_6 r^4(t_0)$ is superimposed on to an increase proportional to $A_4 r^2(t_0)$. As the absolute value of A_6 is greater than A_4, the frequency increase is less than a linear increase.

In the case of a trap truncated at $2r_0$, with the increase of the initial radial-position, the value of the axial secular frequency peak can be greater than that measured with a pure quadrupole ion trap.

5.2.3. Consequence of the secular frequency differences

From the results of the two previous figures, Δ_{1,ω_z} the secular axial-motion frequency difference between an ion trajectory with an initial axial-position $z(t_0) = -1$ mm and one with $z(t_0) = -5$ mm is computed (see Table 2).

The closer to 1 the operating point β_z is, the greater the frequency difference. Δ_{1,ω_z} is about four times lower with a trap truncated at $3r_0$ than with a trap truncated at $2r_0$.

Table 2
Δ_{1,ω_z}, secular axial-motion frequency difference between one ion with initial position $z(t_0) = -1$ mm and an other with -5 mm, both with $x(t_0) = y(t_0) = 0$; Δ_{2,ω_z}, secular axial-motion frequency difference between one ion with initial position $x(t_0) = y(t_0) = 0$ mm and an other with 5 mm, both with $z(t_0) = -2$ mm

	Operating conditions		Δ_{1,ω_z} (Hz)	Δ_{2,ω_z} (Hz)
	V_0 (V)	β_z		
Ion trap truncated at $2r_0$	50	0.217	13.4	9
	100	0.523	25.9	24.1
	145.8	0.929	83.6	103.2
Ion trap truncated at $3r_0$	50	0.217	3.1	2.3
	100	0.523	6	7
	145.8	0.929	19.7	35.5

The other conditions are: $m/z = 130$ u, $\Omega/2\pi = 250$ kHz, $z_0 = 1$ cm, $U_0 = 0$ V, $T_e = T_\Omega = 4$ μs, $N = 20\,000$.

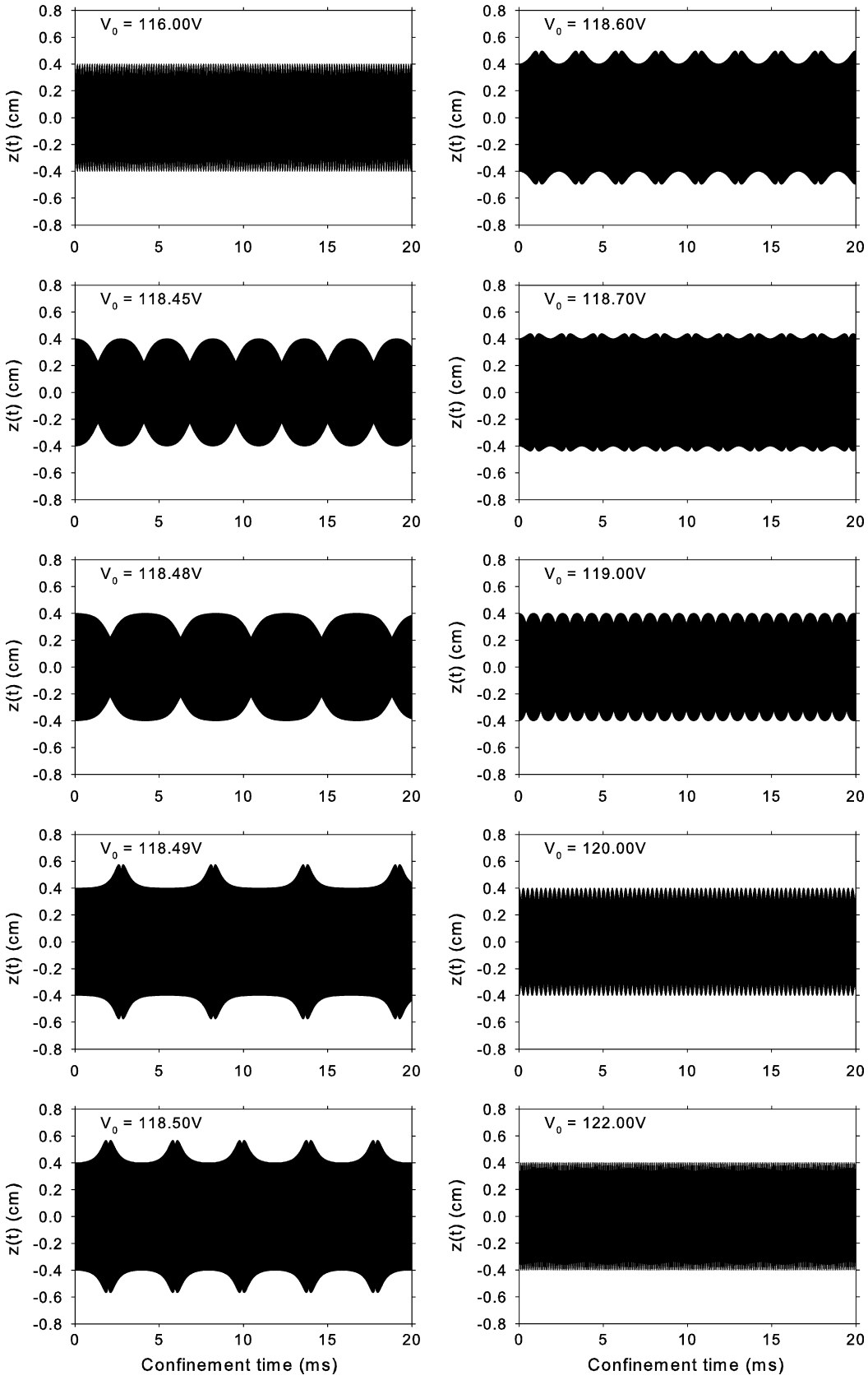

Fig. 4. Axial trajectory vs. V_0 of an ion confined in a stretched trap close to the resonance line $\beta_z = 0.5$. The conditions are: $m/z = 130$ u, $\Omega/2\pi = 250$ kHz, $z_0 = 1$ cm, $U_0 = 0$ V, $T_e = 4$ μs, $N = 20\,000$, $z(t_0) = -4$ mm and $x(t_0) = y(t_0) = 0$ mm.

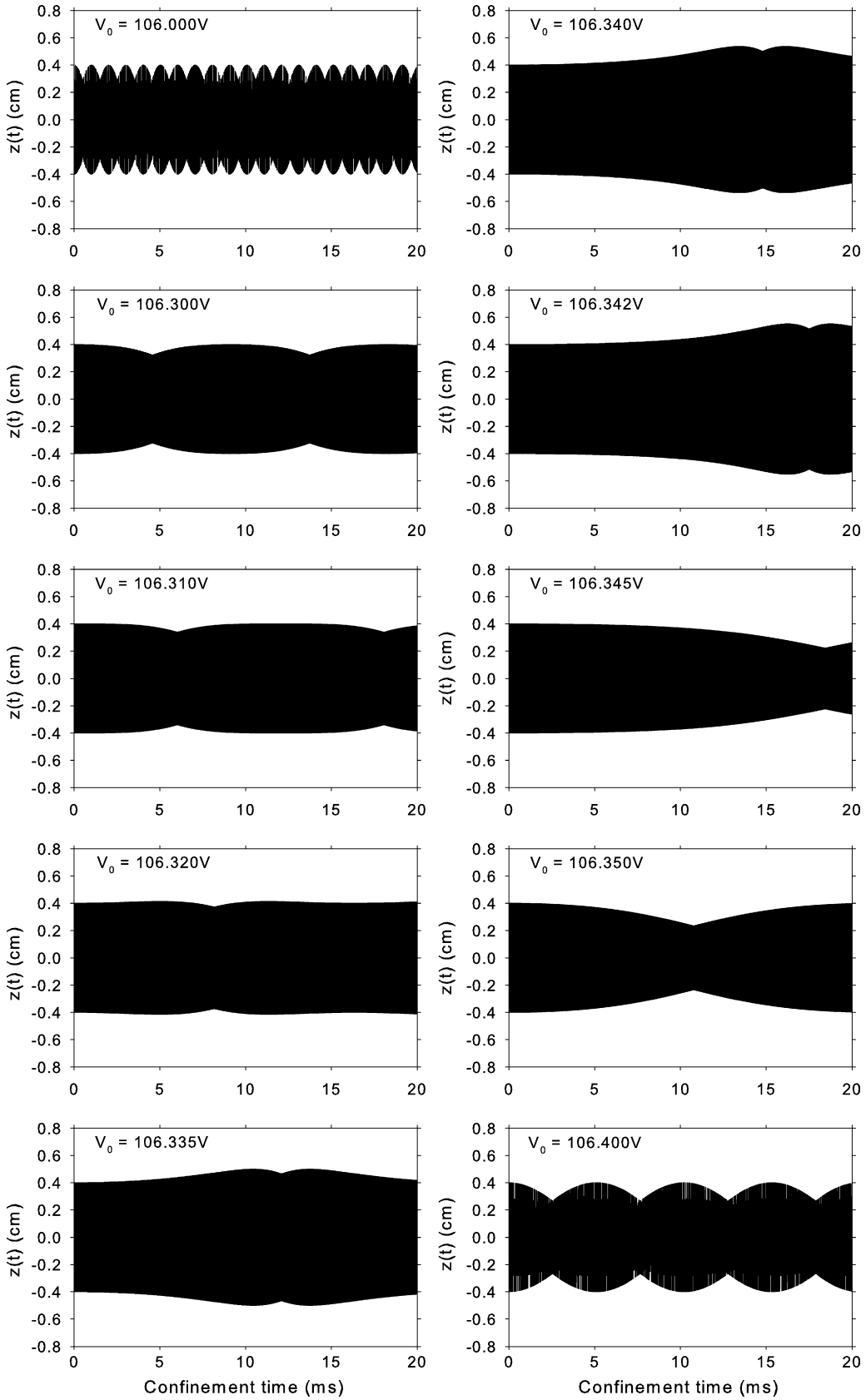

Fig. 5. Axial trajectory vs. V_0 of an ion confined in a trap truncated at $2r_0$ close to the resonance line $\beta_z = 0.5$. The conditions are: $m/z = 130$ u, $\Omega/2\pi = 250$ kHz, $z_0 = 1$ cm, $U_0 = 0$ V, $T_e = 4$ μs, $N = 20\,000$, $z(t_0) = -4$ mm and $x(t_0) = y(t_0) = 0$ mm.

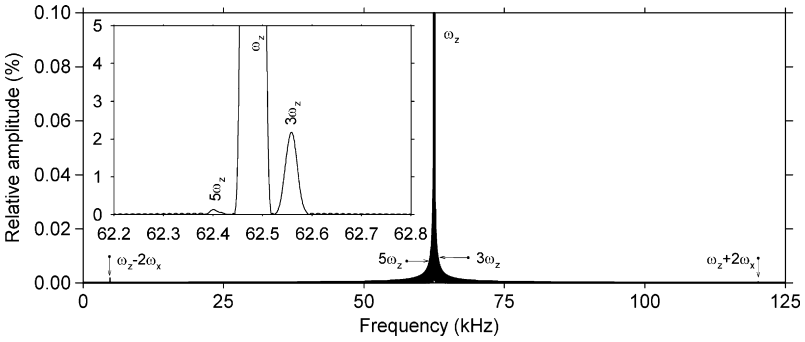

Fig. 6. Axial-motion spectrum of an ion confined in a trap truncated at $3r_0$ for an operating point located under the resonance line $\beta_z = 0.5$. The conditions are: $m/z = 128.47$ u, $\Omega/2\pi = 250$ kHz, $z_0 = 1$ cm, $U_0 = 0$ V, $V_0 = 105$ V, $N = 20\,000$, $z(t_0) = -2$ mm and $x(t_0) = y(t_0) = 2$ mm.

In Table 2, Δ_{2,ω_z} is the secular axial-motion frequency difference between an ion trajectory with an initial radial-position $x(t_0) = y(t_0) = 0$ mm and an ion trajectory with an initial radial-position $x(t_0) = y(t_0) = 5$ mm. A radial difference of 5 mm and an axial difference of 2 mm give about a same frequency difference in the case of a truncated ion trap.

The frequency peak FWHM is equal to about 20 Hz for the power spectrum in these operating conditions. The frequency difference between two ions with different initial conditions (given in Table 2) are sufficiently large to deform the frequency peak or induce a peak splitting in the case of the superimposition of the two ion spectra.

5.3. Influence of two resonance lines

Resonance lines lead to different effects that impair mass analysis. Ion loss can occur and coupling peaks gain amplitude when trap operating point approaches resonance line.

5.3.1. Frequency localisation of the resonance lines

For a set of operating points defined by the pair (a_z, q_z), the values of β_z, β_r and ω_z are computed in the case of a pure quadrupolar trap by the matrix method [33]. The value of ω_z for which the couple (β_z, β_r) fulfils the equation of the resonance line is the frequency of the resonance line. For $U_0 = 0$ and $\Omega/2\pi = 250$ kHz, the resonance line $\beta_z = 0.5$ is localised at the frequency 62.500 kHz and $\beta_z + \beta_r = 1$ at about 87.859 kHz.

The simulations are carried out according to the physical parameters. The frequency of the peak depends on the initial conditions and on the type of non-linearity. Hence, the value of V_0 must be adjusted empirically in order to cause the ion to oscillate with the required frequency.

5.3.2. Motion amplitude and ion loss close to a resonance line

The axial trajectory is computed close to the resonance line $\beta_z = 0.5$. Figs. 4 and 5 show the envelope of this trajectory for

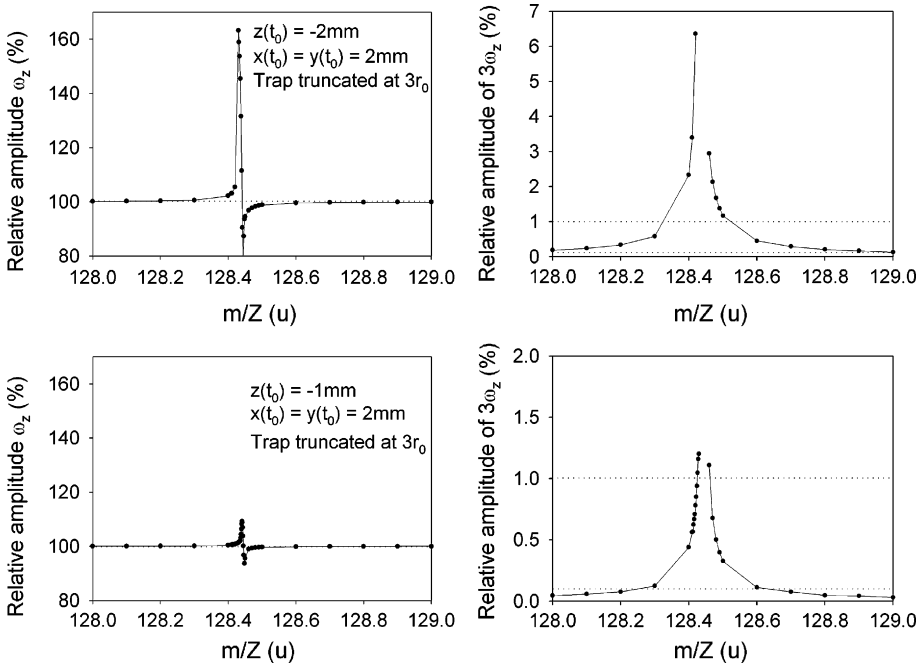

Fig. 7. Amplitude evolution of the peaks ω_z and $3\omega_z$ vs. m/z for a trap truncated at $3r_0$ around the resonance line $\beta_z = 0.5$ and for $z(t_0) = -1$and -2 mm. The other conditions are: $\Omega/2\pi = 250$ kHz, $z_0 = 1$ cm, $U_0 = 0$ V, $V_0 = 105$ V, $T_e = 4$ μs, $N = 20\,000$ and $x(t_0) = y(t_0) = 2$ mm.

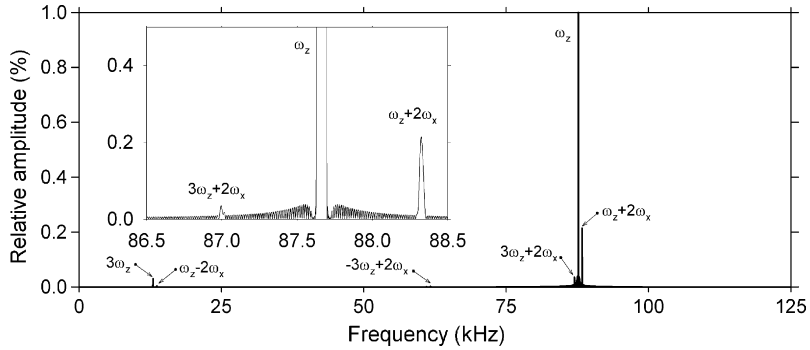

Fig. 8. Axial-motion spectrum of an ion confined in a trap truncated at $3r_0$ for an operating point located under the resonance line $\beta_z + \beta_r = 1$. The conditions are: $m/z = 129.6$ u, $\Omega/2\pi = 250$ kHz, $z_0 = 1$ cm, $U_0 = 0$ V, $V_0 = 134$ V, $N = 20\,000$, $z(t_0) = -2$ mm and $x(t_0) = y(t_0) = 2$ mm.

different operating points by varying V_0 in the case of a stretched trap and a trap truncated at $2r_0$, respectively.

It was proved that the shape of the envelopes is not induced by the particular value of the ratio between the sampling period and the period of the axial secular motion. Smaller values of T_e give an identical shape.

Around the resonance line (for $V_0 < 118.49$ V and $V_0 > 118.70$ V), the axial-trajectory envelope presents beats induced by frequency superimposition. Indeed, the amplitudes of the three main frequency peaks (ω_z, $3\omega_z$ and $5\omega_z$) increase as they approach the resonance line by varying V_0. The maximum amplitude of the trajectory does not exceeded the initial axial-position.

Around and close to the resonance line (from $V_0 = 118.49$ to 118.70 V), one observes the resonance effect: the envelope shape presents periodical extensions greater than the initial axial-position value. When resonance occurs the amplitude

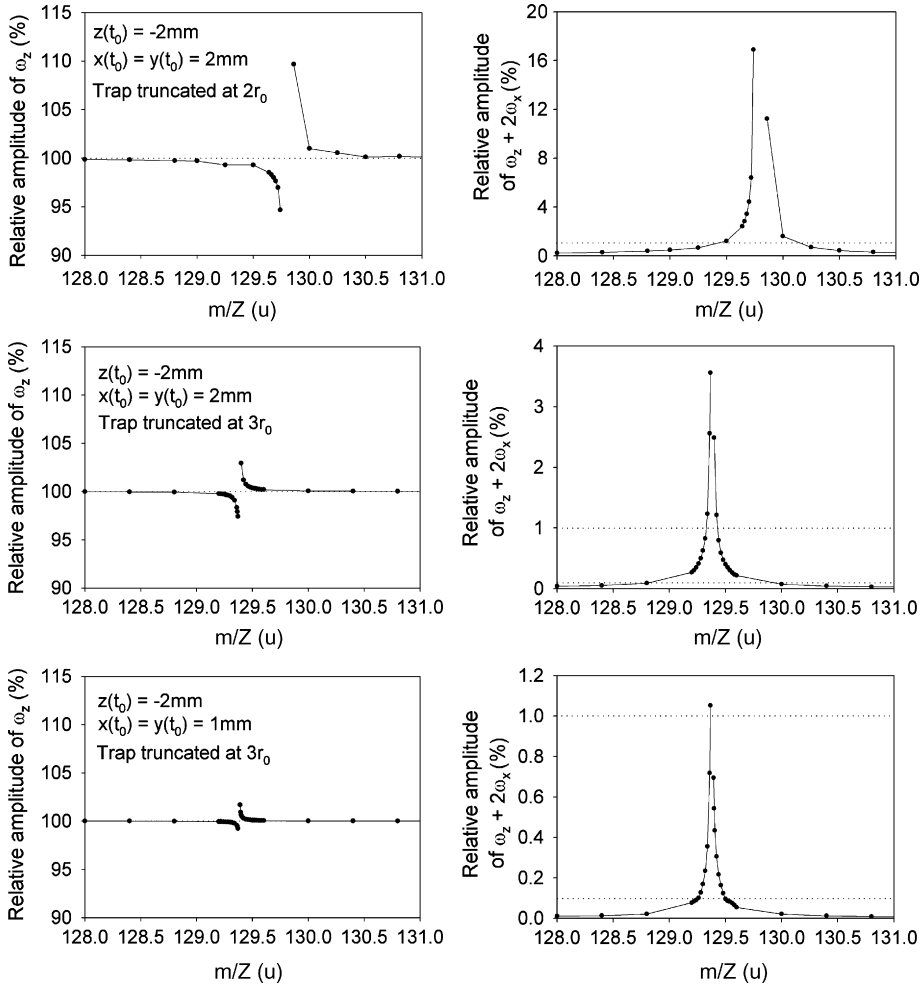

Fig. 9. Amplitude evolution of the peaks ω_z and $\omega_z + 2\omega_x$ vs. m/z for a trap truncated at $2r_0$ and $3r_0$ around the resonance line $\beta_z + \beta_r = 1$ and for $x(t_0) = y(t_0) = 1$ and 2 mm. The other conditions are: $\Omega/2\pi = 250$ kHz, $z_0 = 1$ cm, $U_0 = 0$ V, $V_0 = 134.5$ V for the trap truncated at $2r_0$ and 134 V for the trap truncated at $3r_0$, $T_e = 4$ μs, $N = 20\,000$ and $z(t_0) = -2$ mm.

of the trajectory increases. In this resonance the motion frequency depends on the motion amplitude. Therefore, when the amplitude increases the frequency changes, which moves the operating point out of the resonance. Then the amplitude decreases and the operating point returns to its initial value. The process restarts periodically.

For strong non-linearity (i.e., for the stretched ion trap) the resonance effect occurs in a larger voltage range ($\Delta V_0 \approx 0.365$ V) than for the trap truncated at $2r_0$ ($\Delta V_0 \approx 0.020$ V). With the trap truncated at $3r_0$, amplitude periodical extensions are imperceptible.

For large-amplitude trajectories, the ion can be lost by its reaching one of the two end-cap electrodes for the stretched ion trap and the trap truncated at $2r_0$.

Even with a stretched trap, ion is not ejected under these operating conditions. To the contrary, for the resonance line $\beta_z + \beta_r = 1$, ion ejection occurs with a trap truncated at $3r_0$ and initial conditions $z(t_0) = -1$ mm and $x(t_0) = y(t_0) = 2$ mm.

5.3.3. Axial spectrum near $\beta_z = 0.5$ for a trap truncated at $3r_0$

The ion axial-motion spectrum is shown in Fig. 6 for an operating point located under the resonance line $\beta_z = 0.5$ in the case of a trap truncated at $3r_0$.

With the chosen operating conditions (i.e., a trap truncated at $3r_0$, $z(t_0) = -2$ mm and $x(t_0) = y(t_0) = 2$ mm), the visible peaks are the coupling peaks between the confinement field and:

- the axial direction (induced by A_2): ω_z, $\Omega - \omega_z$, $\Omega + \omega_z$ and $2\Omega - \omega_z$;
- the axial direction (induced by A_4, A_6): $5\omega_z - \Omega$, $\Omega - 3\omega_z$, $3\omega_z$, $2\Omega - 3\omega_z$ and $\Omega + 3\omega_z$;
- the axial and radial directions (induced by A_4): $\omega_z - 2\omega_x$, $\omega_z + 2\omega_x$ and $\Omega - (\omega_z + 2\omega_x)$.

The three main peaks are ω_z, $\Omega - 3\omega_z$ and $5\omega_z - \Omega$. When approaching the resonance line on the left (for example, by increasing V_0), the frequency of the peaks ω_z and $5\omega_z - \Omega$ increases while that of the peak $\Omega - 3\omega_z$ decreases. And the amplitude of these coupling peaks increases too.

In Fig. 6, the sampling period is equal to the period of the confinement field ($T_e = 4$ μs). As a result, due to sampling, the visible peaks are constituted of the superimposition of various coupling peaks for certain sampling orders. The denoted peaks are not located at their true frequency. For example, all the coupling peaks between the confinement field and axial direction ($n\Omega \pm \omega_z$) fold over at the secular axial frequency ω_z: the fold over of the negative frequencies of the sampling order (+1) of the peak $\Omega - \omega_z$ has the frequency value $(+1)\Omega - (\Omega - \omega_z) = \omega_z$, the fold over of the positive frequencies of the sampling order (−1) of the peak $\Omega + \omega_z$ has the frequency value $(-1)\Omega + (\Omega + \omega_z) = \omega_z, \ldots$ The coupling peaks between the confinement field and axial direction $n\Omega \pm 3\omega_z$ fold over at the frequency $\Omega - 3\omega_z$. This peak superimposition is denoted $3\omega_z$ in Fig. 6, as the frequency peaks are referenced according to their generic term. For the operating conditions used in this figure, this secondary peak ($3\omega_z$) has an amplitude greater than 2%. This increases the noise level.

5.3.4. Mass identifying around the resonance line $\beta_z = 0.5$

The confinement potential is chosen to confine ion of $m/z = 130$ u on an operating point located under the resonance line $\beta_z = 0.5$ (Fig. 7). Lower values of m/z ratio are submitted to the resonant effect. Trajectories and resulting spectra are computed for different m/z ratios lower than 130 u. The amplitudes of the main (ω_z) and secondary ($3\omega_z$) peaks are measured.

For the operation conditions used in (Fig. 7) and with a mass step of 0.001 u near the resonance line, one observes periodical trajectories, in other words for each mass there is no ion loss observed, even on the resonance. On the resonance, an overlapping of the two peaks occurs. Consequently, in a given mass range, the amplitudes of the peak $3\omega_z$ is not measured and the amplitudes of the peak ω_z are not significative. For the mass range 128.4–128.5 u, $z(t_0) = -2$ mm and for the mass range 128.432–128.460 u, $z(t_0) = -1$ mm.

The amplitude of the secondary peak impairs mass analysis in the larger mass range. If the minimum detection threshold is set to 1%, the mass range is from 128.32 to 128.52 u for $z(t_0) = -2$ mm and 128.425 to 128.462 u for $z(t_0) = -1$ mm. With a minimum detection threshold set to 0.1%, the damaged mass range is greater than 1 u for $z(t_0) = -2$ mm and about 0.4 u for $z(t_0) = -1$ mm.

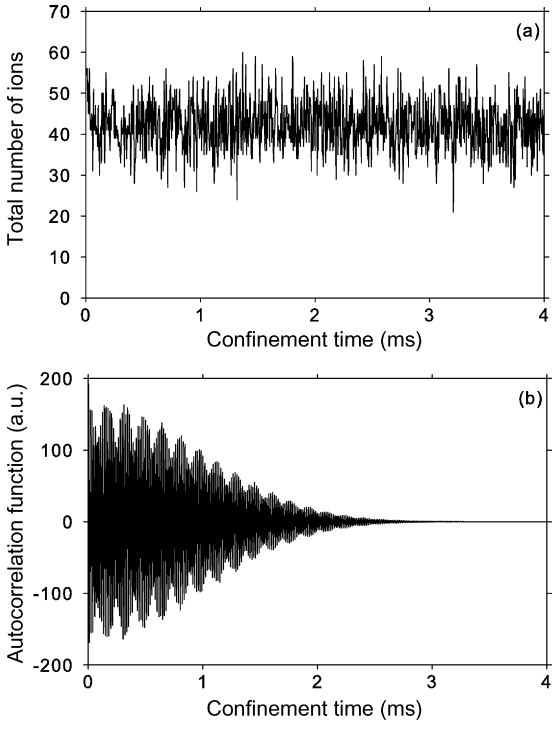

Fig. 10. (a) Total number of detected ions and (b) autocorrelation function vs. confinement time in a trap truncated at $3r_0$ for $N = 1000$. The conditions are: $m/z = 130$ u, $\Omega/2\pi = 250$ kHz, $z_0 = 1$ cm, $U_0 = 0$ V, $V_0 = 108.35$ V, $T_e = T_\Omega = 4$ μs, $\bar{N}_i = 50$ ions, $\bar{x}(t_0) = \bar{y}(t_0) = 0$ mm, $\sigma[x(t_0)] = \sigma[y(t_0)] = 2$ mm, $\bar{v}_x(t_0) = \bar{v}_y(t_0) = 0$ m/s, $\sigma[v_x(t_0)] = \sigma[v_y(t_0)] = 300$ m/s, $\bar{z}(t_0) = -4$ mm, $\sigma[z(t_0)] = 2$ mm, $\bar{v}_z(t_0) = 0$ m/s and $\sigma[v_z(t_0)] = 600$ m/s.

5.3.5. Axial spectrum near the resonance line $\beta_z + \beta_r = 1$

The ion axial-motion spectrum is shown in Fig. 8 for an operating point located under the resonance line $\beta_z + \beta_r = 1$ for a trap truncated at $3r_0$.

This resonance strengthens the coupling peaks between the axial and the two radial directions. The amplitude of the coupling peaks $n\Omega \pm k\omega_z$ diminishes while the amplitude of the coupling peaks $n\Omega \pm (k\omega_z \pm k'\omega_x)$ increases.

For the sampling period $T_e = 4\,\mu s$, the two main peaks, located around ω_z, are formed by the fold over of the peaks: $n\Omega \pm (\omega_z + 2\omega_x)$ and $n\Omega \pm (3\omega_z + 2\omega_x)$. Their are denoted $\omega_z + 2\omega_x$ and $3\omega_z + 2\omega_x$.

5.3.6. Mass identifying around the resonance line $\beta_z + \beta_r = 1$

Confinement potential remains constant: $V_0 = 134.5\,V$ for the trap truncated at $2r_0$ and 134 V for the trap truncated at $3r_0$ (Fig. 7). Operating point for the $m/z = 130\,u$ is located under the resonance line $\beta_z + \beta_r = 1$. Peak amplitudes are computed by the same processing used in Fig. 9 for the resonance line $\beta_z = 0.5$. Here, the resonance line induces ion ejection. Hence, in a given mass range, the amplitude of the peaks ω_z and $\omega_z + 2\omega_x$ cannot be measured.

This resonance line has a stronger effect than the resonance line $\beta_z = 0.5$. For example, we compare the effect of these two resonance lines from Figs. 7 and 9 both obtained with a truncated trap at $3r_0$ and with $x(t_0) = y(t_0) = 2\,mm$ and $z(t_0) = -2\,mm$. Amplitude of the peak ω_z is not significative in a mass range of about 0.1 u around the resonance line $\beta_z = 0.5$ and of about 0.38 u for the resonance line $\beta_z + \beta_r = 1$.

The amplitude of the secondary peak exceeds the value of 1% in a mass range lower than 0.02 u around the resonance line $\beta_z = 0.5$ and about 0.1 u around the resonance line $\beta_z + \beta_r = 1$.

With a lower radial displacement, i.e., $x(t_0) = y(t_0) = 1\,mm$ and $z(t_0) = -2\,mm$, mass analysis will be impaired in a mass range of about 0.1 u around the resonance line $\beta_z + \beta_r = 1$. This mass range corresponds to a defective measure of the peak ω_z. In this mass range, the maximum amplitude for the peak $\omega_z + 2\omega_x$ leads to a minimum threshold of about 0.3%.

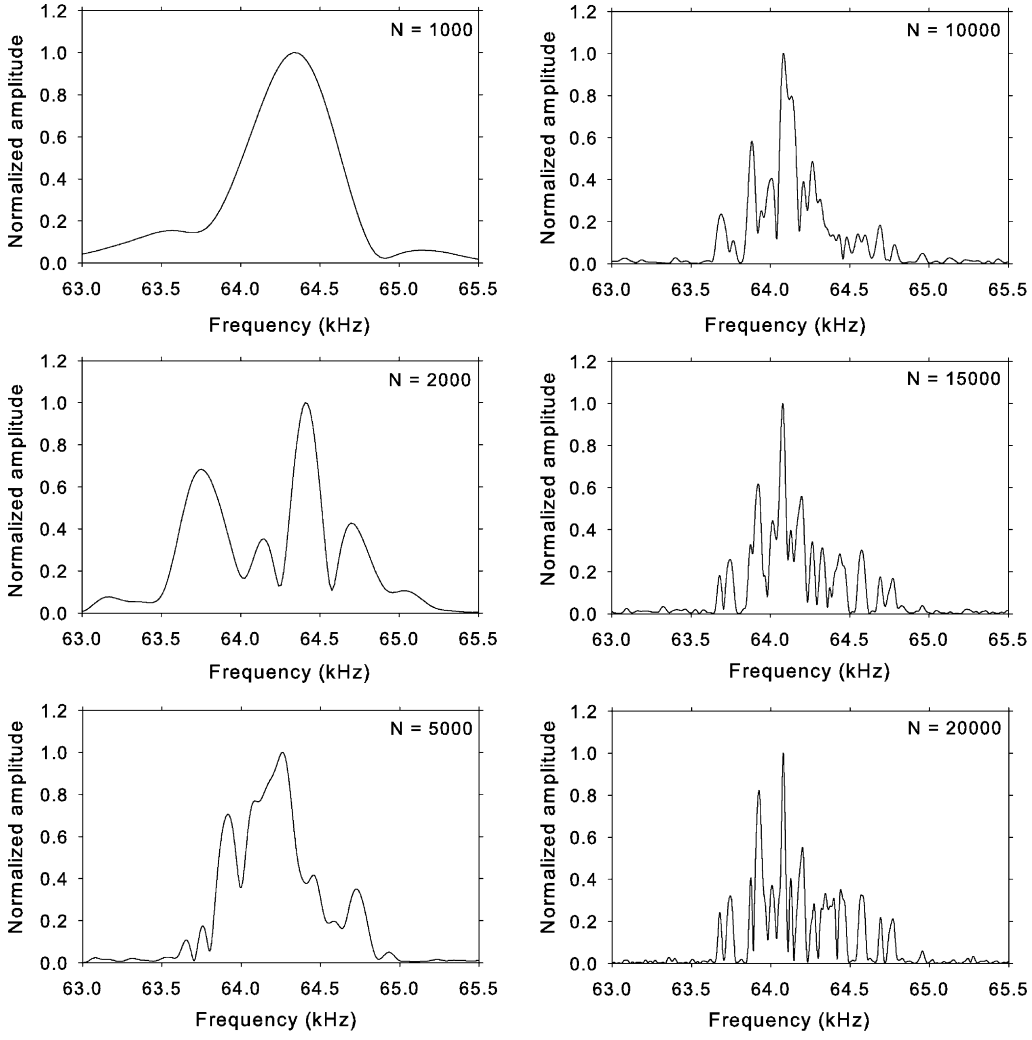

Fig. 11. Evolution of the magnitude spectrum of the axial trajectory of an ion cloud in a stretched trap for certain values of N. The conditions are: $m/z = 130\,u$, $\Omega/2\pi = 250\,kHz$, $z_0 = 1\,cm$, $U_0 = 0\,V$, $V_0 = 121\,V$, $T_e = T_\Omega = 4\,\mu s$, $\bar{N}_i = 50$ ions, $\bar{x}(t_0) = \bar{y}(t_0) = 0\,mm$, $\sigma[x(t_0)] = \sigma[y(t_0)] = 2\,mm$, $\bar{v}_x(t_0) = \bar{v}_y(t_0) = 0\,m/s$, $\sigma[v_x(t_0)] = \sigma[v_y(t_0)] = 300\,m/s$, $\bar{z}(t_0) = -4\,mm$, $\sigma[z(t_0)] = 2\,mm$, $\bar{v}_z(t_0) = 0\,m/s$ and $\sigma[v_z(t_0)] = 600\,m/s$.

5.4. Operating mode preliminaries

The next experimental results will consider an ion cloud spread in positions and velocities at the beginning of the confinement. The instantaneous number of the ions varies depending on the elementary experiment. The spectrum is obtained by carrying out the Fourier transform of an autocorrelation function as a function of the confinement time built from the discrimination of TOF histograms.

In Fig. 10, curves (a) and (b) show the total number of ions as a function of confinement time and the autocorrelation function before, applying the Fourier transform, respectively. These two curves come from the simulation results given later in Fig. 13 with $N = 1000$. The number of detected ions is computed by adding the number of detected pulses for each TOF histogram.

A mean number of 50 ions is chosen for the initial population of the cloud. The fluctuation of the number of ions during confinement time comes from the Poisson draw at each elementary experiment. Initial condition dispersion in position and velocity leads to a very rapid ion loss. The mean number of detected ions is about 41 for a mean initial population of 50. The same cloud of ions confined in a pure quadrupole trap with an equivalent operating point (given the same secular frequency for the ion motion) gives about the same mean number of detected ions. The operating point is chosen far from the influence of a resonance line.

5.5. Influence of non-linearity versus resolution

The magnitude spectrum of the axial trajectory for an ion population with the same mass-to-charge ratio is calculated for: a stretched ion trap (Fig. 11), an ion trap truncated at $2r_0$ (Fig. 12) and an ion trap truncated at $3r_0$ (Fig. 13) for certain values of N.

The value of V_0 is changed in order to keep approximately the same operating point for the three types of non-linearities. The operating point is chosen away from the influence of a resonance line. N evolves between 1000 and 20 000 in order to increase resolution. Each elementary experiment uses a new draw of positions and velocities of the initial ion cloud. To have the same set of initial conditions, the same draw sequence is used in each simulation.

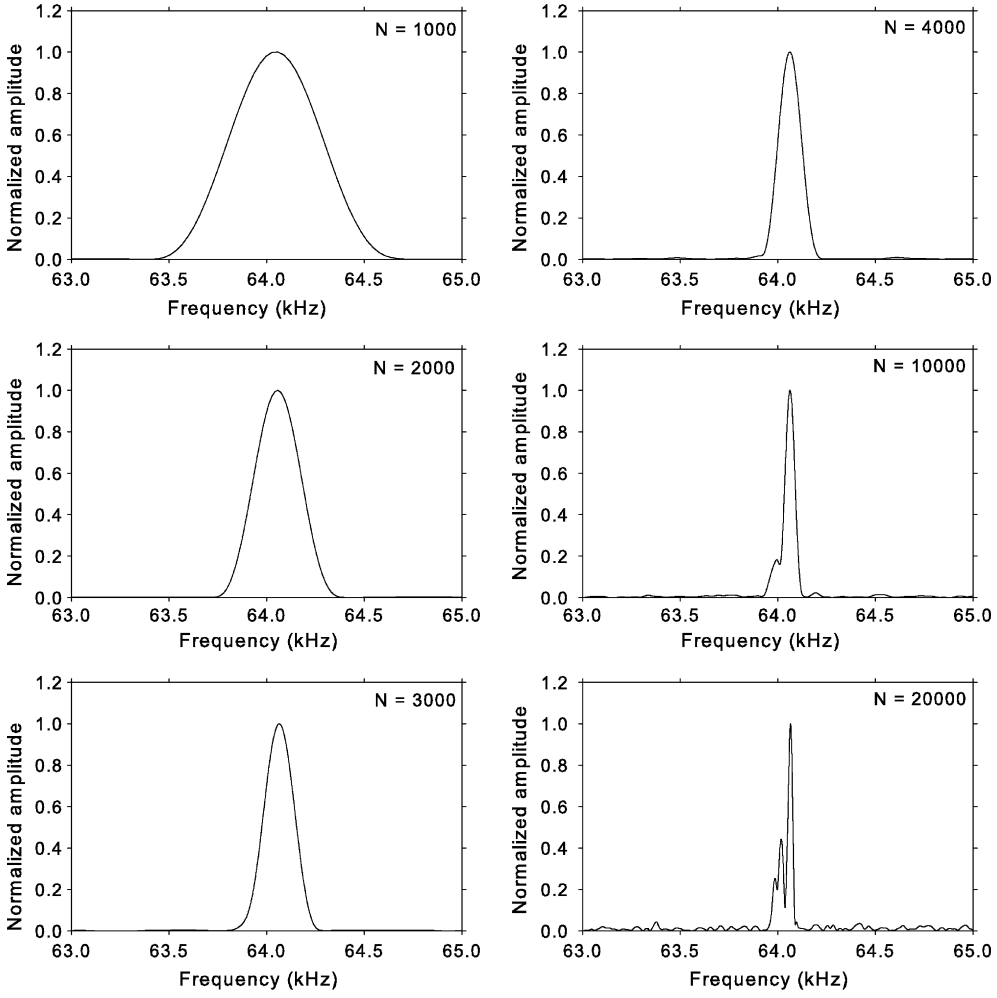

Fig. 12. Evolution of the magnitude spectrum of the axial trajectory of an ion cloud in a trap truncated at $2r_0$ for certain values of N. The conditions are: $m/z = 130$ u, $\Omega/2\pi = 250$ kHz, $z_0 = 1$ cm, $U_0 = 0$ V, $V_0 = 108.4$ V, $T_e = T_\Omega = 4$ μs, $\tilde{N}_i = 50$ ions, $\bar{x}(t_0) = \bar{y}(t_0) = 0$ mm, $\sigma[x(t_0)] = \sigma[y(t_0)] = 2$ mm, $\bar{v}_x(t_0) = \bar{v}_y(t_0) = 0$ m/s, $\sigma[v_x(t_0)] = \sigma[v_y(t_0)] = 300$ m/s, $\bar{z}(t_0) = -4$ mm, $\sigma[z(t_0)] = 2$ mm, $\bar{v}_z(t_0) = 0$ m/s and $\sigma[v_z(t_0)] = 600$ m/s.

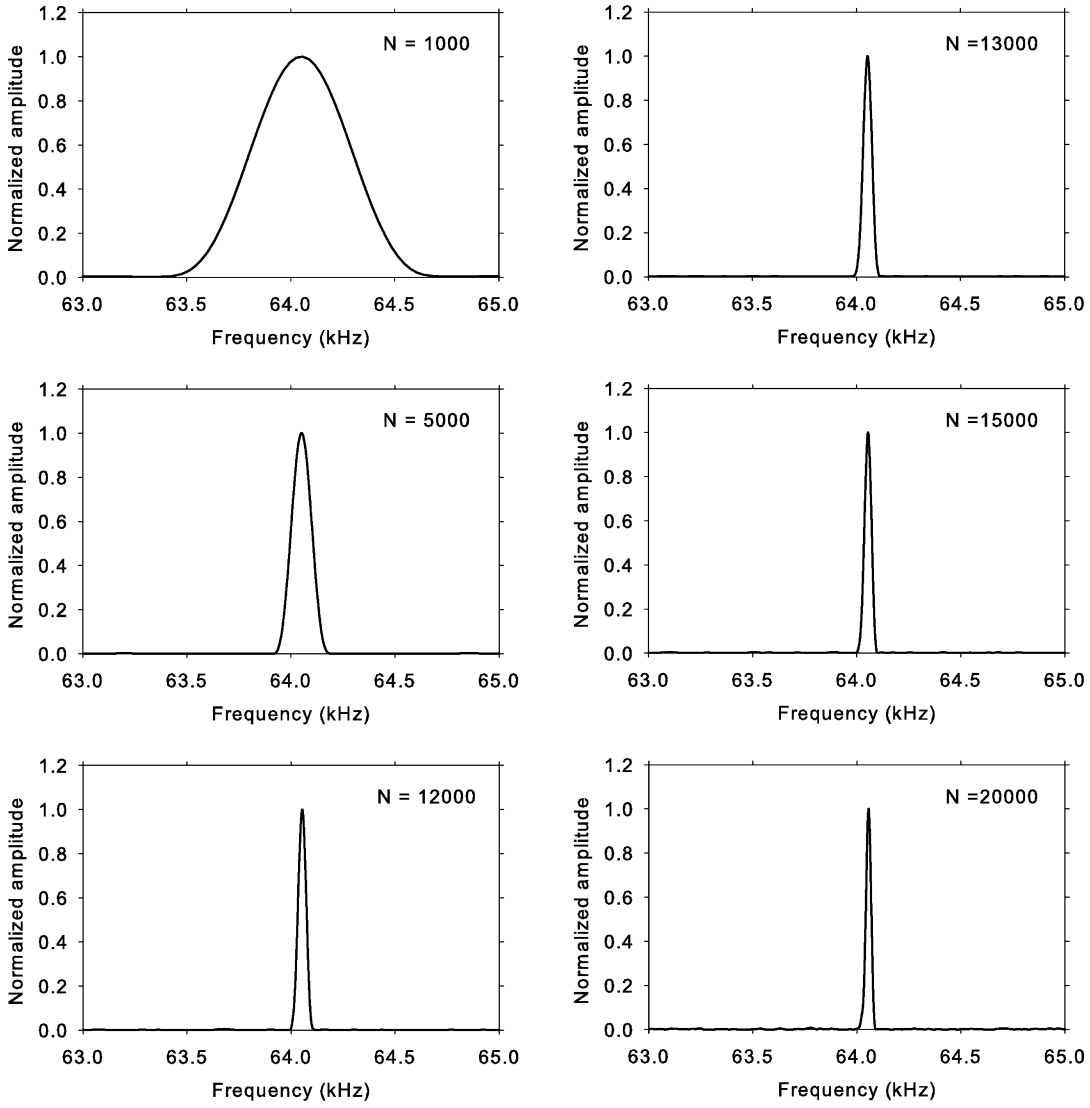

Fig. 13. Evolution of the magnitude spectrum of the axial trajectory of an ion cloud in a trap truncated at $3r_0$ for certains values of N. The conditions are: $m/z = 130$ u, $\Omega/2\pi = 250$ kHz, $z_0 = 1$ cm, $U_0 = 0$ V, $V_0 = 108.35$ V, $T_e = T_\Omega = 4$ μs, $\bar{N}_i = 50$ ions, $\bar{x}(t_0) = \bar{y}(t_0) = 0$ mm, $\sigma[x(t_0)] = \sigma[y(t_0)] = 2$ mm, $\bar{v}_x(t_0) = \bar{v}_y(t_0) = 0$ m/s, $\sigma[v_x(t_0)] = \sigma[v_y(t_0)] = 300$ m/s, $\bar{z}(t_0) = -4$ mm, $\sigma[z(t_0)] = 2$ mm, $\bar{v}_z(t_0) = 0$ m/s and $\sigma[v_z(t_0)] = 600$ m/s.

Fluctuations of the number of ions induce a background frequency noise in the spectrum, but do not affect peak splitting.

In a non-linear trap, each ion evolves with its own axial secular frequency depending on its maximum axial amplitude which is dependent on its initial positions and velocities. Hence, the axial spectrum comprises a superimposition of close-frequency peaks. We look for the maximum limit of the resolution (the limit value for N referred to as N_{lim}) which leads to one peak with the expected shape and full width at half maximum, i.e., which does not reveal the different motion frequency for the ion cloud with the same mass.

For the stretched trap (Fig. 11), with $N = 1000$, the peak shape does not match the expected shape. For higher values of N, several peaks are visible.

For the ion trap truncated at $2r_0$ (Fig. 12), $N_{\text{lim}} \approx 3500$. For this value, $\delta_{1/2,\nu} \approx 160$ Hz (for the magnitude spectrum) and $\delta_{1/2,m/z} \approx 0.256$ u. The resolution limit is about 507 for the mass 130 u.

For the ion trap truncated at $3r_0$ (Fig. 13), $N_{\text{lim}} \approx 11\,500$. In this case, for the power spectrum, $\delta_{1/2,\nu} \approx 35$ Hz, $\delta_{1/2,m/z} \approx 0.056$ u and the mass resolution limit is about 2321 for the mass 130 u.

When $N \leq N_{\text{lim}}$, the value of the peak FWHM agrees with the calculated value from Eq. (11).

When $N > N_{\text{lim}}$, close-frequency small-amplitude peaks generally appear around the main peak. When the resolution is not sufficient to separate them, a widening of the base of the main peak is observed. This agrees with the experimental results where the same behaviour of the spectra was observed [34].

5.6. *Influence of both the initial conditions of the ion cloud and the trap operating point*

Broadening of the ion cloud increases frequency peak splitting. A simulation made in the same conditions as Fig. 13 except

$\sigma[z(t_0)] = 4$ mm leads to $N_{\lim} = 11\,500$ instead of 12 500 with $\sigma[z(t_0)] = 2$ mm.

Initial condition dispersion fixes the lowest limit of the peak FWHM. With the FTQIT operating mode, if V_0 increases, the frequency between two peaks with different masses, Δ_{ω_z}, increases. Hence, resolution increases. However, it was noted in Table 1 that, for one mass, the dispersion of frequency peak (Δ_{1,ω_z}) induced by a dispersion of the initial axial-position increases with V_0.

We must look for the highest optimal value for V_0 that gives the highest resolution without peak splitting.

A simulation is made in the same conditions as Fig. 13 except $V_0 = 138.00$ V. The operating point is located at $\beta_z = 0.74$ between the resonance lines $\beta_z + \beta_r = 1$ and $2\beta_z - 2\beta_r = 1$ corresponding (for $U_0 = 0$) to the secular axial frequency values 87.94 and 102.63 kHz, respectively. One obtains $N_{\lim} = 7500$. In consequence, for the power spectrum, the lowest value for $\delta_{1/2,v}$ is about 53 Hz, the lowest value for $\delta_{1/2,m/z}$ is about 0.04 u and the mass resolution is about 3250.

With this operating point, mass resolution is better than for $V_0 = 108.35$ V (Fig. 13). Frequency FWHM ($\delta_{1/2,v}$) is lower but frequency difference between two peaks (Δ_{ω_z}) is greater.

6. Conclusion

Non-linearities have two main harmful effects for the FTQIT operating mode.

Amplitudes and frequency of the confinement potential remain constant during mass analysis. Consequently, the first effect is to impair mass analysis on mass range for that the operating point sustains the influence of a resonance line.

On the resonance line $\beta_z = 0.5$, periodical extensions of the motion amplitude are observed in a range lower than 30 mV for V_0 in the case of a trap truncated at $2r_0$. This can lead to ion loss for the ions having large amplitudes. Ion loss occurs for the resonance line $\beta_z + \beta_r = 1$, even with a trap truncated at $3r_0$ and small maximum amplitudes (with initial positions $x(t_0) = y(t_0) = 1$ mm and $z(t_0) = -2$ mm and null initial velocities).

Main peak amplitude varies around resonance line making it defective for mass quantification. Coupling peaks gain amplitude that reduces signal-to-noise ratio or increases the minimum detection threshold.

For example, with a trap truncated at $3r_0$ and with the maximum amplitude equal to 2 mm on axial direction and 2 mm on both radial directions, the damaged mass range is about 0.1 u around the resonance line $\beta_z = 0.5$. For the same experimental conditions mass range is about 0.38 u for the resonance line $\beta_z + \beta_r = 1$. With a lower maximum amplitude of the motion (1 mm for the axial direction) mass analysis is impaired on a mass range of about 0.028 u for the resonance line $\beta_z = 0.5$.

Experimental results have shown an amplitude rundown on the resonance line $\beta_z = 0.5$ for isotopic Xe^+ ions (see Fig. 4 of [34]). Here, the trap is truncated at $2r_0$ and has a poor electrode alignment leading to a non-axial-symmetric trap.

To minimise this effect, mass analysis may be performed on small mass ranges (around 10 u) between two strong resonance lines.

The second harmful effect comes from the dependence of the secular frequency on the maximum amplitude of the motion during confinement. The studied operating mode requires a de-centred ion cloud as peak amplitude of the spectrum is an increasing function of the maximum amplitude during confinement. In experiment, it is difficult to have both an ion cloud that is de-centred and concentrated at the initial confinement time. In consequence, even far from a resonance line, ions are also submitted to a non-linear effect leading to peak splitting. This limits resolution.

Frequency motion depends on the maximum amplitude which is approximately equivalent to the initial position of the ions with an initial velocity that is null. With a truncated ion trap, the secular axial frequency decreases with the increasing of the maximum amplitude of the axial trajectory, while it increases with the increasing of the maximum amplitude of the radial trajectory. For example, for an operating point β_z around 0.5, a difference of 4 mm for $z(t_0)$ induces a secular axial frequency difference of about 26 Hz for a trap truncated at $2r_0$ and about 6 Hz for a trap truncated at $3r_0$.

In spectra coming from the operating mode used in this work, resolution collapses very quickly with the increase of the degree of non-linearity. For example, with a trap truncated at $2r_0$ the resolution is four times lower than with a trap truncated at $3r_0$. Mass resolution (for the mass 130 u) is 507 with a trap truncated at $2r_0$ and 2321 with a trap truncated at $3r_0$ for an operating point located at $\beta_z \approx 0.51$. As a result, the mass spectrometer prototype will integrate a new ion trap truncated at 3 r_0 to reach a better resolution.

In the operating mode used here, if V_0 increases, the frequency between two peaks with different masses increases. However, for one given mass, the dispersion of frequency peaks induced by a dispersion of initial conditions also increases. This reduces the value of $N_{\lim}$. For an operating point located at $\beta_z \approx 0.74$ ($V_0 = 138$ V), $N_{\lim} = 7500$, but mass resolution increases compared with that obtained for $\beta_z \approx 0.51$. Mass resolution is equal to about 3250.

Simulation uses a Gaussian draw for all initial positions and velocities. For the axial direction, when $\bar{z}(t_0) = -4$ mm and $\sigma[z(t_0)] = 2$ mm, 95% of the ions have an axial-position between 0 and -8 mm. This induces a large distribution of frequency.

A better ion resolution was obtained in experiments compared to simulation results. With a trap truncated at $2r_0$, the mass resolution is about 4000 for the operating point $\beta_z \approx 0.58$ and $\beta_r \approx 0.25$ and $N_{\lim}$ is greater than 8000 [34].

At the initial time of the confinement, ion cloud dispersion and localisation in position and velocity are difficult to established in experiments. In simulation, these conditions in position and velocity are chosen independent and are drawn from Gaussian laws. This is not representative of the experimental initial conditions. In the device used in the experiment either ion cloud dispersion is lower or the ion cloud is less de-centred for the same dispersion.

With an external ion source, two parameters are fundamental: (1) the turn back point (a de-centred axial-position in the trap with zero velocity) in the trap and (2) the injec-

tion ion TOF (the time to go from the source to the turn back point).

The turn back point depends on the potentials applied to the trap electrodes to slow down the ions during injection and on the potential and kinetic energies of the ions at the creation. The present source is "large", i.e., its volume is greater than 1 cm^3. Hence, neither the initial energies nor the position of the turn back point are not well known.

The ion TOF fixes the injection duration and the beginning of the confinement. If the dynamics of the ions is not well known it is difficult to determine the injection ion TOF value. A small error for this parameter leads to unwanted initial conditions: for example, an ion cloud with a mean axial velocity different from zero.

With this injection mode, it is difficult to know the initial conditions for the ion cloud. Another injection mode will be studied in order to cancel the influence of the injection time and reduce the initial condition dispersions.

References

[1] F. von Bush, W. Paul, Z. Phys. 164 (1961) 581.
[2] P.H. Dawson, N.R. Whetten, Int. J. Mass Spectrom. Ion Proc. 2 (1969) 45.
[3] P.H. Dawson, N.R. Whetten, Int. J. Mass Spectrom. Ion Proc. 3 (1969) 1.
[4] Y. Wang, J. Franzen, Int. J. Mass Spectrom. Ion Proc. 112 (1992) 167.
[5] Y. Wang, J. Franzen, K.P. Wanczek, Int. J. Mass Spectrom. Ion Proc. 124 (1993) 125.
[6] Y. Wang, J. Franzen, Int. J. Mass Spectrom. Ion Proc. 132 (1994) 155.
[7] J. Franzen, Int. J. Mass Spectrom. Ion Proc. 125 (1993) 165.
[8] J. Franzen, Int. J. Mass Spectrom. Ion Proc. 130 (1994) 15.
[9] R. Alheit, C. Henning, R. Morgenstern, F. Vedel, G. Werth, Appl. Phys. B 61 (1995) 277.
[10] X.Z. Chu, M. Holzki, R. Alheit, G. Werth, Int. J. Mass Spectrom. Ion Proc. 173 (1998) 107.
[11] A.A. Makarov, Anal. Chem. 68 (1996) 4257.
[12] W. Mo, M.L. Langfor, J.F.J. Todd, Rapid Commun. Mass Spectrom. 9 (1995) 107.
[13] F. Guidugli, P. Traldi, Rapid Commun. Mass Spectrom. 5 (1991) 343.
[14] K.L. Morand, S.A. Lammert, R.G. Cooks, Rapid Commun. Mass Spectrom. 5 (1991) 491.
[15] D.M. Eades, R.A. Yost, Rapid Commun. Mass Spectrom. 6 (1992) 573.
[16] J. Louris, G. Stafford, J. Syka, D. Taylor, Proceedings of the 40th Conference on Mass Spectrometry and Allied Topics, ASMS East Lansing, Washington, DC, 1992, p. 1003.
[17] R.E. March, F.A. Londry, R.L. Alfred, Org. Mass Spectrom. 27 (1992) 1151.
[18] J. Walz, I. Siemers, M. Schubert, W. Neuhauser, R. Blatt, Europhys. Lett. 21 (1993) 183.
[19] J. Franzen, Int. J. Mass Spectrom. Ion Proc. 106 (1991) 63.
[20] M. Splendore, E. Marquette, J. Oppenheimer, C. Huston, G. Wells, Int. J. Mass Spectrom. 190/191 (1999) 129.
[21] D.M. Eades, J.V. Johnson, R.A. Yost, J. Am. Soc. Mass Spectrom. 4 (1993) 917.
[22] R.E. Kaiser, R.G. Cooks, G.C. Stafford, J.E.P. Syka, P.H. Hemberger Jr., Int. J. Mass Spectrom. Ion Proc. 106 (1991) 79.
[23] Y. Zerega, P. Perrier, M. Carette, Meas. Sci. Technol. 14 (2003) 323.
[24] M. Carette, P. Perrier, Y. Zerega, G. Brincourt, J.C. Payan, J. Andre, Int. J. Mass Spectrom. Ion Proc. 171 (1997) 253.
[25] A.G. Marshall, F.R. Verdun, Fourier Transforms in NMR, Optical, and Mass Spectrometry: A User's Handbook, Elsevier, Amsterdam, 1990, p. 80.
[26] Y. Zerega, J. Andre, G. Brincourt, R. Catella, Int. J. Mass Spectrom. Ion Proc. 135 (1994) 155.
[27] Y. Zerega, S. Bouzid, A. Janulyte, R. Hallegatte, M. Carette, Meas. Sci. Technol. 16 (2005) 1201.
[28] J. Franzen, R.H. Gabling, M. Schubert, Y. Wang, Chapter 3: Nonlinear ion trap, in: R.E. March, J.F.J. Todd (Eds.), Practical Aspects of Ion Trap Mass Spectrometry, vol. 1, CRC Press, Boca Raton, 1995, See fig., pp. 76–77 and the explanations.
[29] L. Landau, E. Lifchitz, Mécanique, 4ème éd., Editions MIR, Moscow, 1981, p. 137.
[30] S. Sevugarajan, A.G. Menon, Int. J. Mass Spectrom. 189 (1999) 53.
[31] P. Perrier, T. NGuema, M. Carette, J. Andre, Y. Zerega, G. Brincourt, R. Catella, Int. J. Mass Spectrom. Ion Proc. 171 (1997) 19.
[32] W.R. Plass, H. Li, R.G. Cooks, Int. J. Mass Spectrom. 228 (2003) 237.
[33] M. Baril, R. LE, P. Marchand, Int. J. Mass Spectrom. Ion Proc. 98 (1990) 87.
[34] M. Carette, Y. Zerega, J. Mass Spectrom. 41 (2005) 71.